https://dx.doi.org/10.1016/j.ultras.2021.106607

Imaging Damage in Plate Waveguides Using Frequency-domain Multiple Signal Classification (F-MUSIC)

Xiongbin Yang[a], Kai Wang[b], Pengyu Zhou[a], Lei Xu[a], and Zhongqing Su[a, c, d*]

[a] Department of Mechanical Engineering
The Hong Kong Polytechnic University, Kowloon, Hong Kong SAR

[b] School of Aerospace Engineering, Xiamen University, Xiamen 361005, PR China

[c] The Hong Kong Polytechnic University Shenzhen Research Institute,
Shenzhen 518057, PR China

[d] School of Astronautics,
Northwestern Polytechnical University, Xi'an 710072, PR China

submitted to ***Ultrasonics***

(first submitted on 19 August 2021; revised and re-submitted on 20 September 2021)

[*] To whom correspondence should be addressed. Tel.: +852-2766-7818, Fax: +852-2365-4703, Email: Zhongqing.Su@polyu.edu.hk (Prof. Zhongqing SU, *PhD*)

Abstract

Earlier, an ameliorated MUSIC (Am-MUSIC) algorithm is developed by the authors [1], aimed at expanding conventional MUSIC algorithm from linear array-facilitated nondestructive evaluation to *in situ* health monitoring with a sparse sensor network. Yet, Am-MUSIC leaves a twofold issue to be improved: i) the signal representation equation is constructed at each pixel across the inspection region, incurring high computational cost; and ii) the algorithm is applicable to monochromatic excitation only, ignoring signal features scattered out of the excitation frequency band which also carry information on structural integrity. With this motivation, a multiple-damage-scattered wavefield model is developed, with which the signal representation equation is constructed in the frequency domain, avoiding computationally expensive pixel-based calculation – referred to as *frequency-domain MUSIC* (F-MUSIC). F-MUSIC quantifies the orthogonal attributes between the signal subspace and noise subspace inherent in signal representation equation, and generates a full spatial spectrum of the inspected sample to visualize damage. Modeling in the frequency domain endows F-MUSIC with the capacity to fuse rich information scattered in a broad band and therefore enhance imaging precision. Both simulation and experiment are performed to validate F-MUSIC when used for imaging single and multiple sites of damage in an isotropic plate waveguide with a sparse sensor network. Results accentuate that effectiveness of F-MUSIC is not limited by the quantity of damage, and imaging precision is not downgraded due to the use of a highly sparse sensor network – a challenging task for conventional MUSIC algorithm to fulfil.

Keywords**:** ultrasonic imaging; guided ultrasonic waves; multiple signal classification (MUSIC); sparse sensor network; frequency domain analysis

1. Introduction

Multiple signal classification (MUSIC) algorithm is a proven array processing technique for guided wave-based damage characterization [2-6]. Instead of using straightforward wave features such as time-of-flight or signal amplitude [7-12], MUSIC is an eigen-structure approach making use of the orthogonality of subspaces extracted from wave signals [13-16]. Stepinski and Engholm [17] are among those who first demonstrated the use of the MUSIC algorithm for estimating the direction of arrival (DOA) of an incoming wave in acoustic emission. As an extension of that study, Yang *et al* [18, 19] determined the direction of impact-induced acoustic waves accurately using MUSIC in conjunction with a linear sensor array. The approach, however, failed to precisely locate the impact site, as the approach is based on the far-field hypothesis which simplifies the impact-emanated wave as a plane wavefront when the wave arrives at the array – it is not true for a waveguide of small dimensions. To circumvent this limitation, Zhong *et al* [3] developed a near-field MUSIC algorithm on the basis of Taylor expansion theory, in which an incoming wave was deemed as a spherical wavefront. This method was validated by locating damage in a real composite oil tank, showing potentials to improve localization accuracy. Extending this study and also taking into account other impact-induced wave components out of the excitation frequency range, Yuan *et al* [20] proposed a single frequency component-based re-estimated MUSIC (SFCBR-MUSIC) algorithm with Shannon wavelet transform, showing proven capability of localizing impact to a composite wing box in aircraft. Conventional MUSIC was revamped by Zhong *et al* [21] based on 2D near-field assumption and Gerschgorin discs theorem, and this revamped MUSIC algorithm facilitated detection of multiple sites of damage.

In addition to these parametric studies concerning passive impact localization, MUSIC-based detection has also been extended to active damage identification. Bao *et al* [22] combined transmitter beamforming and weighted imaging with MUSIC, with which the severity of corrosion in aluminum plates was assessed using actively generated waves, in conjunction with the use of a dual array consisting of two linear sensor groups. Zuo *et al* [23] presented a model-based MUSIC algorithm by calculating the cross-correlation function between the modeled wave scattering signals and measured residual signals, to identify a mass added to a composite laminate, though material anisotropy of the composites and discrepancy of wave velocities in different propagation directions were not considered in modeling. To compensate for the anisotropy of composites, Bao *et al* [24, 25] developed an updated MUSIC algorithm, taking into account the effect of both the sensor localization error and the sensor phase error due to material anisotropy, whereby to enhance damage localization precision.

Despite proven effectiveness, MUSIC-driven damage identification is usually restricted to the use of a linear array featuring a dense configuration of transmitter elements with a sufficiently small and uniform element pitch. Approaches in this category barely provide full inspection coverage, presenting downgraded beamforming capability at azimuth angles close to 0° and 180°, as a result of which the damage in an inspection region of [0, 30°] or [150°, 180°] may be overridden [26]. To circumvent such deficiency, an ameliorated MUSIC (Am-MUSIC) algorithm was developed by the authors in an earlier study [1], in which the signal representation matrix is manipulated at each pixel using the excitation signal series, instead of the scattered signal series. Am-MUSIC algorithm does not necessarily demand the use of a linear phased array, and instead it is compatible with a sparse sensor array. In the sparse sensor array, individual transducers can be positioned arbitrarily. The Am-MUSIC yields a full spatial spectrum of the inspected sample, and damage in the sample, if any, can thus be visualized in the spectrum.

However, the flexibility in sensor array configuration bestowed by the Am-MUSIC algorithm is at the cost of higher computational expense (compared with conventional MUSIC algorithms), because the signal representation matrix is calculated at each pixel across the entire inspection region. In addition, Am-MUSIC algorithm is manipulated in the time domain within a narrowed frequency band, at which the monochromatic wave is excited. Such manipulation discards wave components in a captured signal that are out of the excitation frequency range, irrespective of the fact that these wave components also carry rich information on damage in the sample [27, 28].

Aimed at exploiting the merits of Am-MUSIC algorithm earlier developed (particularly its flexibility in configuring a sensor network) but surmounting deficiency that the algorithm remains, a frequency-domain MUSIC algorithm (F-MUSIC) is developed, in conjunction with the use of a sparse sensor network with arbitrarily positioned transducers. Distinct from Am-MUSIC, F-MUSIC constructs the signal representation equation over the frequency domain, rather than at each pixel in the spatial domain, based on a multiple-damage-scattered wavefield model. F-MUSIC quantifies the orthogonal attributes between the signal subspace and noise subspace inherent in signal representation equation, and produces a full spatial spectrum of the inspected sample to pinpoint damage. The accuracy of F-MUSIC is examined via simulation and experiment, in which single and multiple sites of damage in a plate waveguide are imaged with a sparse sensor network.

2. Principle of Methodology

Consider a monochronic Lamb wave guided by a plate waveguide, $f(t)$. Upon propagating the distance of *d*, without considering the attenuation, the received signal, $r(t)$, is governed by

$$r(t) = \int_{-\infty}^{\infty} F(\omega) e^{-ik(\omega)d} \exp^{i\omega t} \, d\omega \,, \tag{1}$$

where $F(\omega)$ is the Fourier transform of $f(t)$ in the frequency domain, t the time, ω the angular frequency, i the imaginary unit, and $k(\omega)$ the wavenumber of the Lamb wave ($k(\omega)=\omega/c_p(\omega)$, where $c_p(\omega)$ is the phase velocity). Applying Fourier transform on Eq. (1), $r(t)$ in the frequency domain, $R(\omega)$, is obtained by

$$R(\omega) = F(\omega)\exp^{-ik(\omega)d} = F(\omega)\exp^{-i\omega d/c_p(\omega)}. \tag{2}$$

Assuming a wave scatterer (e.g., damage) in the waveguide, the scatterer can be modeled as a secondary wave source to scatter incoming $f(t)$ and interfere with the original wavefield of signal $f(t)$; and the scattered wavefield $R^{\text{scattered}}(\omega)$ in the frequency domain can be defined by modulating the original wavefield with a scattering coefficient related to the scatterer, as

$$R^{\text{scattered}}(\omega) = \alpha(\omega)F(\omega)\exp^{-i\omega d^{\text{scattered}}/c_p(\omega)}, \tag{3}$$

where $\alpha(\omega)$ is the scattering coefficient in the frequency domain, and $d^{\text{scattered}}$ is the distance from the excitation source to the scatterer and then to the wave receiver.

Discuss a sparse sensor network with Q piezoelectric lead zirconate titanate (PZT) wafers (labelled as PZT-*1*, …, PZT-*i*, …, PZT-*Q*) ($i = 1, 2, \ldots, Q$) surface-mounted on the plate waveguide, as shown schematically in **Fig. 1**. With an arbitrary position on the waveguide, each wafer functions as a wave transmitter and a wave receiver as well. Thus, this sensor network renders $M = Q(Q-1)$ transmitter–receiver paths, and the m^{th} transmitter–receiver path ($m = 1, 2, \ldots, M$) links PZT-*i* (as wave transmitter) and PZT-*j* (as wave receiver).

For an intact waveguide, the wave signal, captured by the m^{th} transmitter–receiver path (denoted with $r_m^{\text{measured-intact}}(t)$), is the direct arrival wave $r_m^{\text{direct}}(t)$, boundary-reflection wave $r_m^{\text{boundary-reflection}}(t)$ with incoherent noise $w_m^{\text{measured-intact}}(t)$,as

$$r_m^{\text{measured-intact}}(t) = r_m^{\text{direct}}(t) + r_m^{\text{boundary-reflection}}(t) + w_m^{\text{measured-intact}}(t), \quad \left(m = 1, 2, \ldots, M\right). \tag{4}$$

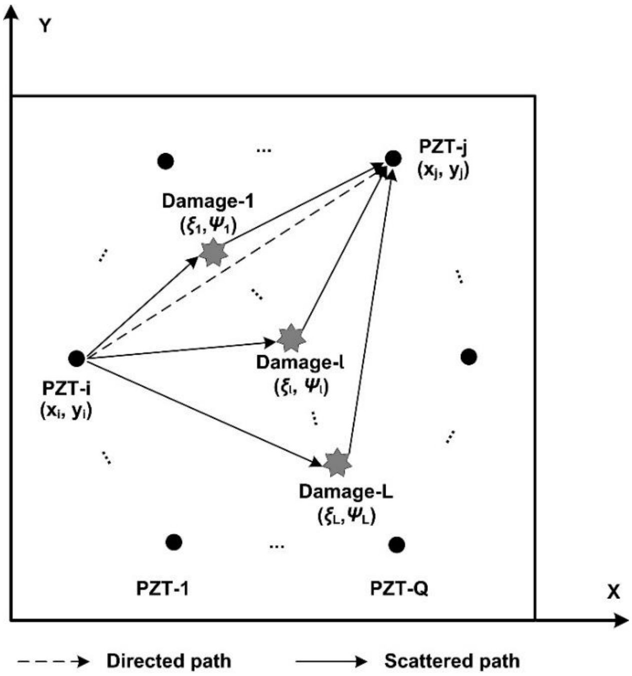

Fig. 1. A plate waveguide with a sparse sensor network of *Q* PZT wafers and *L* damage sites.

Assume that up to L damage sites co-exist in the waveguide which are respectively located at $(\xi_1,\psi_1),\ldots,(\xi_l,\psi_l),\ldots,(\xi_L,\psi_L)$. Ignoring mode conversion and multiple reflection among damage sites, the wave signal captured by the same transmitter-receiver path, $r_m^{\text{measured-damage}}(t)$, embraces the direct arrival waves $r_m^{\text{direct}}(t)$, boundary-reflection wave $r_m^{\text{boundary-reflection}}(t)$, damage-scattered waves $r_m^{\text{scattered},l}(t),\left(l=1,2,\ldots,L\right)$ from all damage sites, and the incoherent noise $w_m^{\text{measured-damage}}(t)$, as

$$r_m^{\text{measured-damage}}(t)=r_m^{\text{direct}}(t)+r_m^{\text{boundary-reflection}}(t)+\sum_{l=1}^{L}r_m^{\text{scattered},l}(t)+w_m^{\text{measured-damage}}(t),\quad\left(m=1,2,\ldots,M\right), \tag{5}$$

where $r_m^{\text{scattered},l}(t)$ represents the wave signal that propagates from PZT-*i* (as wave transmitter) to the l^{th} damage site and then to PZT-*j* (as wave receiver).

Benchmarking against the intact waveguide, one has,

$$r_m^{\text{measured-damage}}(t) - r_m^{\text{measured-intact}}(t) = \sum_{l=1}^{L} r_m^{\text{scattered},l}(t) + w_m(t) = r_m^{\text{residual}}(t), \qquad (m = 1, 2, \ldots, M) \quad (6)$$

where $w_m(t)$ signifies the difference between two noise terms, $w_m^{\text{measured-damage}}(t) - w_m^{\text{measured-intact}}(t)$. To facilitate discussion in what follows, the term, $\sum_{l=1}^{L} r_m^{\text{scattered},l}(t) + e_m(t)$, is referred to as the m^{th} residual signal $r_m^{\text{residual}}(t)$. Applying Fourier transform on Eq. (6) and substituting Eqs. (3) to (6), the m^{th} residual signal in the frequency domain, $R_m^{\text{residual}}(\omega)$, is obtained as

$$R_m^{\text{residual}}(\omega) = \sum_{l=1}^{L} \alpha^l(\omega) F(\omega) \exp^{-i\omega d_m^l / c_p(\omega)} + W_m(\omega), \qquad (m = 1, 2, \ldots, M) \quad (7)$$

where $\alpha^l(\omega)$ denotes the scattering coefficient for the l^{th} damage site within the inspection region; $d_m^l = \sqrt{(\xi_l - x_i)^2 + (\psi_l - y_i)^2} + \sqrt{(\xi_l - x_j)^2 + (\psi_l - y_j)^2}$, which represents the distance from the i^{th} wave transmitter to the l^{th} damage and then to the j^{th} wave receiver; $W_m(\omega)$ is the Fourier counterpart of $w_m(t)$ in the frequency domain.

Defining that $\hat{F}_l(\omega) = \alpha^l(\omega) F(\omega)$ and $a_m^l(\omega) = \exp^{-i\omega d_m^l / c_p(\omega)}$, both of which are related to the l^{th} damage site, the residual signal $R_m^{\text{residual}}(\omega)$ can be rewritten, in the frequency domain, as

$$R_m^{\text{residual}}(\omega) = \sum_{l=1}^{L} a_m^l(\omega) \hat{F}_l(\omega) + W_m(\omega). \qquad (m = 1, 2, \ldots, M) \quad (8)$$

Extending the above manipulation to all the available M transmitter–receiver paths in the sensor network, it has

$$\mathbf{R}^{\text{residual}}(\omega) = \begin{bmatrix} R_1^{\text{residual}}(\omega) \\ \vdots \\ R_m^{\text{residual}}(\omega) \\ \vdots \\ R_M^{\text{residual}}(\omega) \end{bmatrix}_{M\times 1} = \begin{bmatrix} a_1^1(\omega) & \cdots & a_1^l(\omega) & \cdots & a_1^L(\omega) \\ \vdots & & \vdots & & \vdots \\ a_m^1(\omega) & \cdots & a_m^l(\omega) & \cdots & a_m^L(\omega) \\ \vdots & & \vdots & & \vdots \\ a_M^1(\omega) & \cdots & a_M^l(\omega) & \cdots & a_M^L(\omega) \end{bmatrix}_{M\times L} \begin{bmatrix} \hat{F}_1(\omega) \\ \vdots \\ \hat{F}_l(\omega) \\ \vdots \\ \hat{F}_L(\omega) \end{bmatrix}_{L\times 1} + \begin{bmatrix} W_1(\omega) \\ \vdots \\ W_m(\omega) \\ \vdots \\ W_M(\omega) \end{bmatrix}_{M\times 1}. \quad (9)$$

$\mathbf{R}^{\text{residual}}(\omega)=[R_1^{\text{residual}}(\omega),\cdots,R_m^{\text{residual}}(\omega),\cdots,R_M^{\text{residual}}(\omega)]^H$ is the residual signal vector for the entire sensor network. Defining that $\mathbf{a}_l(\omega)=[a_1^l(\omega),\cdots,a_m^l(\omega),\cdots,a_M^l(\omega)]^H$ as the steering vector for the l^{th} damage site, $\mathbf{A}(\omega)=[\mathbf{a}_1(\omega),\cdots,\mathbf{a}_l(\omega),\cdots,\mathbf{a}_L(\omega)]$ as the steering vector dictionary for all damage sites, $\mathbf{F}(\omega)$=$[\hat{F}_1(\omega),\cdots,\hat{F}_l(\omega),\cdots,\hat{F}_L(\omega)]^H$ as the excitation signal vector, and $\mathbf{W}(\omega)=[W_1(\omega),\cdots,W_m(\omega),\cdots,W_M(\omega)]^H$ as the noise term, Eq. (9) is

$$\mathbf{R}^{\text{residual}}(\omega)=\mathbf{A}(\omega)\mathbf{F}(\omega)+\mathbf{W}(\omega)\,. \tag{10}$$

Equation (10) defines all wave signals received by the entire sensor network, containing multiple damage-scattered wave components. It is referred to as a *multiple-damage-scattered wavefield model* over the frequency domain. With this model, the residual signal series can be expressed with the excitation signal series, which is independent of the location of a wave receiver. It is such merit that allows arbitrarily positioning sensors in the sensor network – difficult to fulfill by conventional MUSIC algorithms which are largely bound up with the use of a dense, linear array with a uniform element pitch. Equation (10) also serves as the theoretical cornerstone for the F-MUSIC, as detailed as below.

Recalling the conventional MUSIC algorithm, the covariance matrix $\mathbf{C}(\omega)$ of the residual signal vector $\mathbf{R}^{\text{residual}}(\omega)$ is defined as

$$\begin{aligned}\mathbf{C}(\omega)&=E\left[\mathbf{R}^{\text{residual}}(\omega)\cdot\mathbf{R}^{\text{residual}}(\omega)^H\right]\\&=\mathbf{A}(\omega)E\left[\mathbf{F}(\omega)\cdot\mathbf{F}(\omega)^H\right]\mathbf{A}(\omega)^H+\mathbf{A}(\omega)E\left[\mathbf{F}(\omega)\cdot\mathbf{W}(\omega)^H\right]\\&\quad+E\left[\mathbf{W}(\omega)\cdot\mathbf{F}(\omega)^H\right]\mathbf{A}(\omega)^H+E\left[\mathbf{W}(\omega)\cdot\mathbf{W}(\omega)^H\right],\end{aligned} \tag{11}$$

where $E[\cdot]$ is covariance computation and the superscript H the complex conjugate transpose. As the source signal is un-correlated to a noise signal, both $E\left[\mathbf{F}(\omega)\cdot\mathbf{W}(\omega)^H\right]$ and $E\left[\mathbf{W}(\omega)\cdot\mathbf{F}(\omega)^H\right]$ retreat to zero. The noise, $\mathbf{W}(\omega)$, is commonly a Gaussian white noise which satisfies

$E\left[\mathbf{W}(\omega)\cdot\mathbf{W}(\omega)^H\right]=\sigma^2\mathbf{I}(\omega)$, where σ^2 is noise power and $\mathbf{I}(\omega)$ the identity matrix. Therefore, Eq. (11) can be rewritten as

$$\mathbf{C}(\omega)=\mathbf{A}(\omega)\mathbf{C}_{\mathbf{f}}(\omega)\mathbf{A}(\omega)^H+\sigma^2\mathbf{I}(\omega), \tag{12}$$

where $\mathbf{C}_{\mathbf{f}}(\omega)=E\left[\mathbf{F}(\omega)\cdot\mathbf{F}(\omega)^H\right]$, denoting the covariance matrix of the source signal.

Applied with eigenvalue decomposition, the covariance matrix $\mathbf{C}(\omega)$ in Eq. (12) is decomposed into two orthogonal subspaces, viz., signal subspace and noise subspace, as

$$\mathbf{C}(\omega)=\mathbf{U}(\omega)\mathbf{\Sigma}(\omega)\mathbf{U}(\omega)^H=\mathbf{U}_S(\omega)\mathbf{\Sigma}_S(\omega)\mathbf{U}_S(\omega)^H+\mathbf{U}_N(\omega)\mathbf{\Sigma}_N(\omega)\mathbf{U}_N(\omega)^H, \tag{13}$$

where $\mathbf{U}(\omega)=[\mu_1(\omega),\mu_2(\omega),\cdots,\mu_M(\omega)]$ (the eigenvectors), and $\mathbf{\Sigma}(\omega)=\mathrm{diag}[\lambda_1,\lambda_2,...,\lambda_M]$ (the eigenvalues with $\lambda_1>\lambda_2>\cdots>\lambda_j>\lambda_{j+1}=\lambda_{j+2}=\cdots=\lambda_M=\sigma^2$). The number of damage sites can be predicted by counting the number of eigenvalues $\lambda_1,\lambda_2,\cdots,\lambda_j$, which is equal to *j*. The signal subspace $\mathbf{U}_S(\omega)=[\mu_1(\omega),\mu_2(\omega),\cdots,\mu_j(\omega)]$ is spanned by the eigenvectors corresponding to the *j* largest eigenvalues $\mathbf{\Sigma}_S(\omega)=\mathrm{diag}[\lambda_1,\lambda_2,...,\lambda_j]$; the noise subspace $\mathbf{U}_N(\omega)=[\mu_{j+1}(\omega),\mu_{j+1}(\omega),\cdots,\mu_M(\omega)]$ is spanned by those eigenvectors corresponding to the remaining eigenvalues $\mathbf{\Sigma}_N(\omega)=\mathrm{diag}[\lambda_{j+1},\lambda_{j+2},...,\lambda_M]$.

Multiplying $\mathbf{U}_N(\omega)$ with $\mathbf{C}(\omega)$ in Eq. (12) results in

$$\mathbf{C}(\omega)\mathbf{U}_N(\omega)=\mathbf{A}(\omega)\mathbf{C}_{\mathbf{f}}(\omega)\mathbf{A}(\omega)^H\mathbf{U}_N(\omega)+\sigma^2\mathbf{U}_N(\omega). \tag{14}$$

As $\mathbf{C}(\omega)\mathbf{U}_N(\omega)=\sigma^2\mathbf{U}_N(\omega)$ (according to Eq. (13)), substituting $\sigma^2\mathbf{U}_N(\omega)$ into Eq. (14) leads to

$$\mathbf{A}(\omega)\mathbf{C}_{\mathbf{f}}(\omega)\mathbf{A}(\omega)^H\mathbf{U}_N(\omega)=\mathbf{0}. \tag{15}$$

Due to the full rank of $\mathbf{C}_{\mathbf{f}}(\omega)$, Eq. (15) can be simplified as

$$\mathbf{A}(\omega)^H\mathbf{U}_N(\omega)=[\mathbf{a}_1(\omega)^H\mathbf{U}_N(\omega),\cdots,\mathbf{a}_l(\omega)^H\mathbf{U}_N(\omega),\cdots,\mathbf{a}_L(\omega)^H\mathbf{U}_N(\omega)]=\mathbf{0}. \tag{16}$$

Equation (16) indicates that the steering vectors at a damage site are orthogonal with regard to the noise subspace, because $\mathbf{a}_l(\omega)^H \mathbf{U}_N(\omega) = \mathbf{0}$.

With that, the F-MUSIC algorithm is defined in terms of the degree of orthogonality between the steering vector at each pixel and the noise subspace $\mathbf{U}_N(\omega)$, as

$$P_{F-MUSIC}(x, y, \omega) = \frac{1}{\left\| \mathbf{a}_{xy}(\omega)^H \mathbf{U}_N(\omega) \right\|^2} = \frac{1}{\mathbf{a}_{xy}(\omega)^H \mathbf{U}_N(\omega) \mathbf{U}_N(\omega)^H \mathbf{a}_{xy}(\omega)}, \tag{17}$$

where

$$\mathbf{a}_{xy}(\omega) = [\exp^{-i\omega d_{xy}^1 / c_p(\omega)}, \cdots, \exp^{-i\omega d_{xy}^m / c_p(\omega)}, \cdots, \exp^{-i\omega d_{xy}^M / c_p(\omega)}]^H,$$

$$d_{xy}^m = \sqrt{(x - x_i)^2 + (y - y_i)^2} + \sqrt{(x - x_j)^2 + (y - y_j)^2}.$$

By varying (x, y) in Eq. (17), the entire inspection region of the sample under inspection is scanned, and a spatial spectrum is obtained. In the presence of damage at a particular location, the steering vector $\mathbf{a}_{xy}(\omega)$ is orthogonal to the noise subspace $\mathbf{U}_N(\omega)$, as a result of which the denominator of Eq. (17) tends to be zero, resulting in a steep peak in the spatial spectrum, to indicate the damage presence and its location. It is noteworthy that on the basis of the multiple-damage-scattered wavefield model, the eigenvalue decomposition in Eq. (13) is calculated only once, and then the calculated $\mathbf{U}_N(\omega)$ is applicable to all pixels. It is such a feature of the F-MUSIC algorithm that avoids time-consuming pixel-based calculation – a demerit of the AM-MUSIC algorithm developed earlier [1], and remarkably lowers the computational costs.

On the other hand, the residual wave signals, $\mathbf{R}^{\text{residual}}(\omega)$, are distributed over a broad band ($\boldsymbol{\omega}$) rather than confined at the frequency of wave excitation. The broadband signals embrace rich information on damage or material degradation along wave propagation path. With this in mind, the F-MUSIC algorithm is further refined by integrating the calculation conducted by Eq. (17) over a broad frequency band ($\boldsymbol{\omega}$), as

$$P_{F-MUSIC}(x,y)=\frac{1}{\sum_{\omega\in\boldsymbol{\omega}}\left|\frac{1}{P_{F-MUSIC}(x,y,\omega)}\right|}. \tag{18}$$

Compared with conventional MUSIC algorithms manipulated in the time domain solely at the monochromatic excitation frequency, Eq. (18) suggests that F-MUSIC algorithm, based on the analysis of the multiple-damage-scattered wavefield over the frequency domain, fuses rich wave components over a broad frequency band, consequently enhancing imaging precision (to be demonstrated in what follows).

3. Numerical Validation

3.1 Modeling and Results

To verify the developed multiple-damage-scattered wavefield model and proposed F-MUSIC algorithm, numerical simulation is implemented first. A homogeneous, isotropic plate (density: ρ=2700 kg/m^3; Young modulus: E=71 GPa; Poisson's ratio: ν=0.33; dimension: 300 mm × 300 mm × 2 mm) is modeled. Eight PZT wafers (labelled as P1, P2, …, P8) that are on the surface of the plate form a sparse sensor network for wave generation and acquisition (a total of $8(8-1)=56$ sensing path), as illustrated schematically in **Fig. 2**.

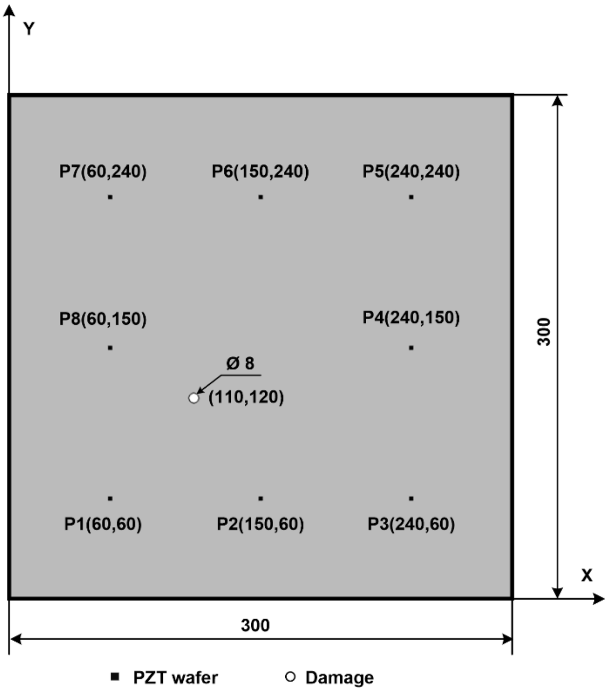

Fig. 2. Schematic of a plate waveguide in simulation with a sparse sensor network (all dimensions in mm).

Two scenarios are comparatively modeled: one is the benchmark that is free of damage, and the other contains a through-hole of a diameter of 8 mm at (110 mm, 120 mm). Allowing for sensitivity and excitability, a 5-cycle Hanning windowed toneburst at 200 kHz, **Fig. 3**, is generated by each PZT wafer in turn, and in the meantime the rest wafers serve as wave receivers to capture S_0 mode Lamb wave signals in a time window of 150 μs. In **Fig. 3** the bandwidth of the excitation, centralized at 200 kHz, is observed to span from 100 to 300 kHz. The 56 sets of residual signals, $r_m^{\text{residual}}(t), \left(m=1,2,\ldots,56\right)$ in Eq. (6), are obtained and shown in a waterfall view in **Fig. 4**.

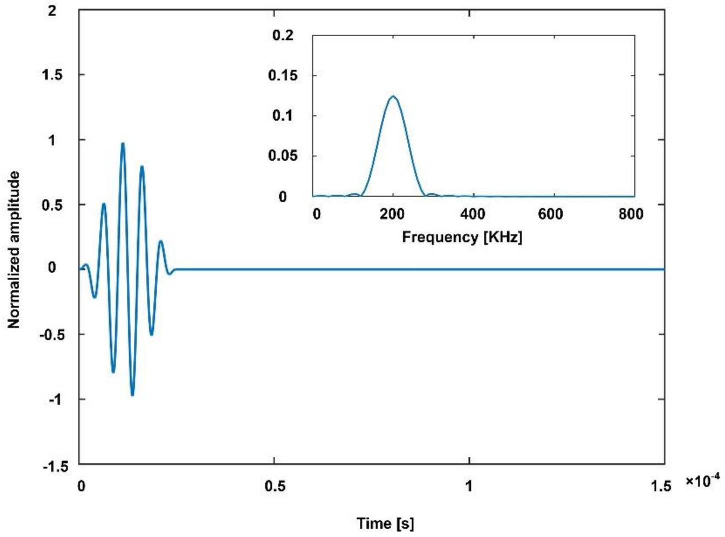

Fig. 3. Excitation signal and frequency domain spectrum.

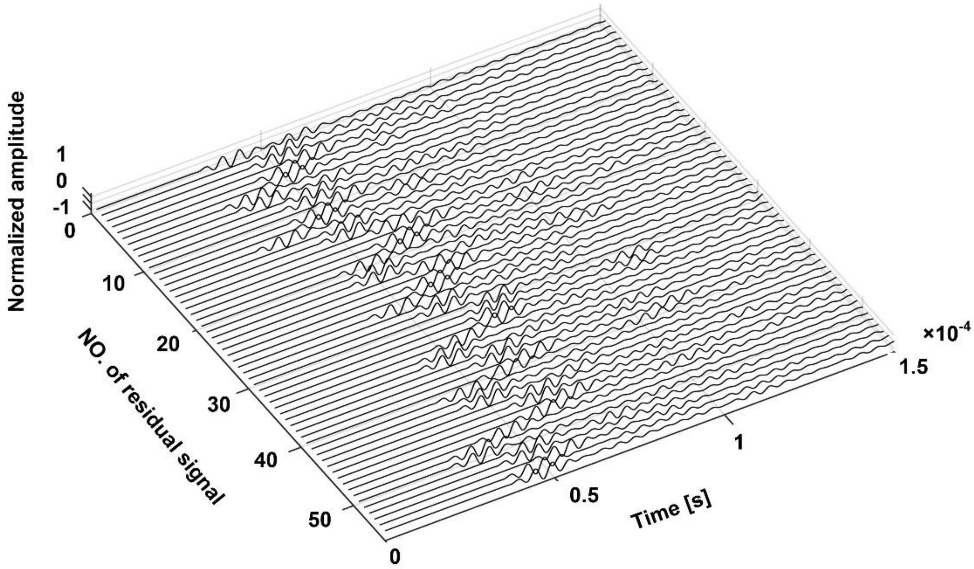

Fig. 4. Waterfall view of 56 sets of residual signals.

Applying the F-MUSIC algorithm on all residual signals at the excitation frequency of 200 kHz using Eq. (17), the spatial spectrum of the plate containing the through-hole is displayed in **Fig. 5(a)**, in which, however, the damage can barely be visualized. Further, upon taking into account wave components scattered in the whole frequency band of excitation (100–300 kHz, as observed in **Fig. 3**) with Eq. (18), the re-constructed image is shown in **Fig. 5(b)**, which explicitly indicates the damage site and depicts the damage geometry with reduced artifacts, compared with **Fig. 5(a)**.

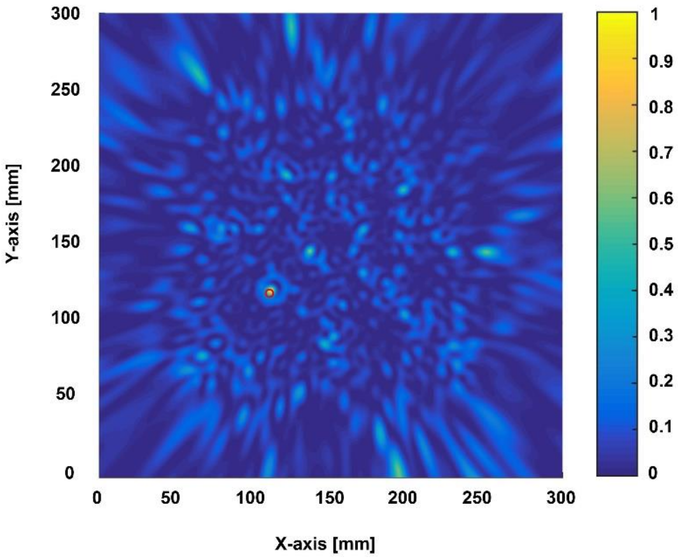

(a)

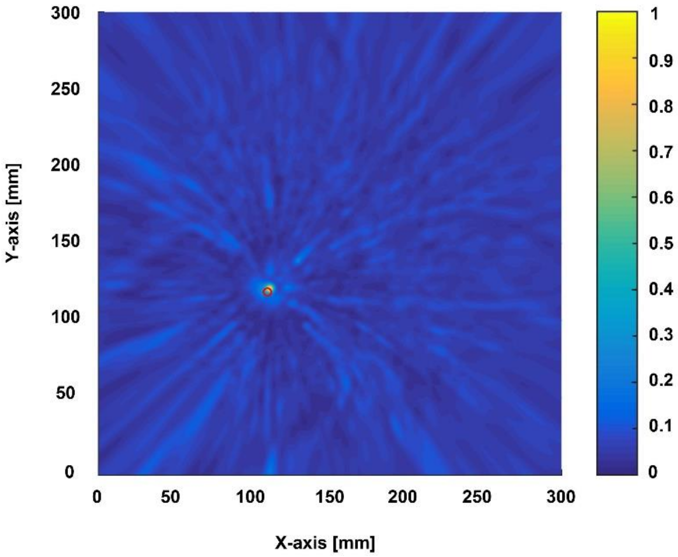

(b)

Fig. 5. Spatial spectra obtained with F-MUSIC algorithm: (a) at the excitation frequency of 200 kHz; and (b) over the whole excitation band of 100–300 kHz (red ‘o’: actual damage).

3.2 Discussion

Comparison with Conventional MUSIC Algorithm

The conventional MUSIC algorithm [3, 21, 29] is recalled to image the same damage in the above scenario for comparison. To this end, seven PZT wafers are configured in a linear array as wave receivers, **Fig. 6**, along with another PZT wafer at (150 mm, 240 mm) as wave transmitter. The image constructed using the conventional MUSIC algorithm is presented in **Fig. 7**, failing to pinpoint and size the through-hole. In addition, an elongation artifact is spotted along the scanning direction toward the damage, which is related to the point-spread function of the liner array at the location of the damage [3, 20-24].

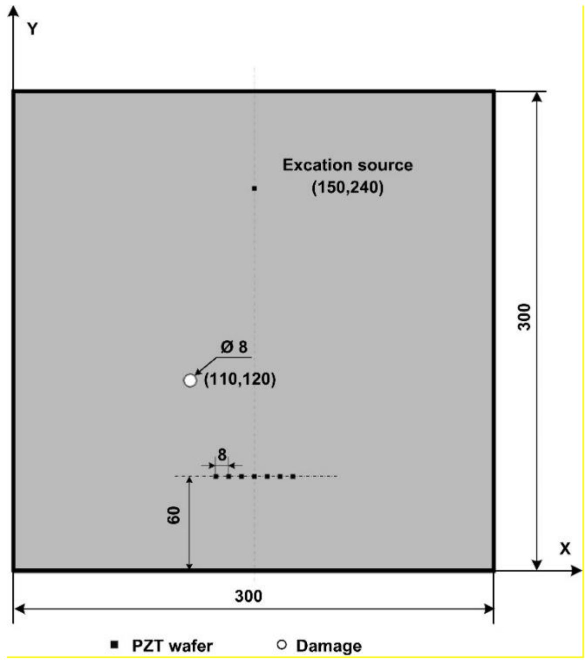

Fig. 6. Schematic of a plate waveguide in simulation with a linear sensor array to implement conventional MUSIC algorithm (all dimensions in mm).

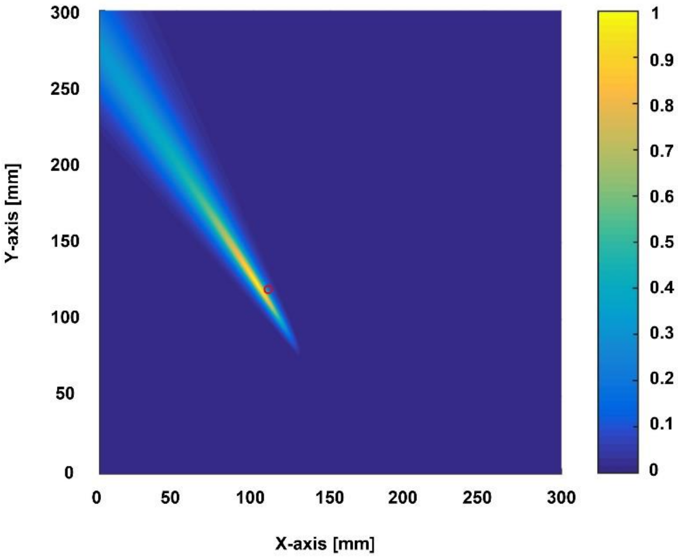

Fig. 7. Spatial spectrum obtained with conventional MUSIC algorithm (red 'o': actual damage).

Different Patterns of Sensor Distribution in Sparse Sensor Network

To examine the performance of F-MUSIC algorithm when the sensors are arranged in different patterns in the sparse sensor network, parametric studies respectively using six PZT wafers (namely, P1, P2, P4, P5, P6, P8) and using four PZT wafers (P2, P4, P6, P8), **Fig. 2**, are conducted, and correspondingly imaged spatial spectra are in **Figs. 8** and **9**, respectively. Comparison with the spectrum in **Fig. 5(b)** constructed when eight PZT wafers are used, these results obtained using partial sensors of the sparse sensor network with different sensor distribution patterns still show a high degree of detectability, and this implies the high flexibility in sensor network configuration endowed by the F-MUSIC algorithm: not only in number of sensors, but in sensor distribution.

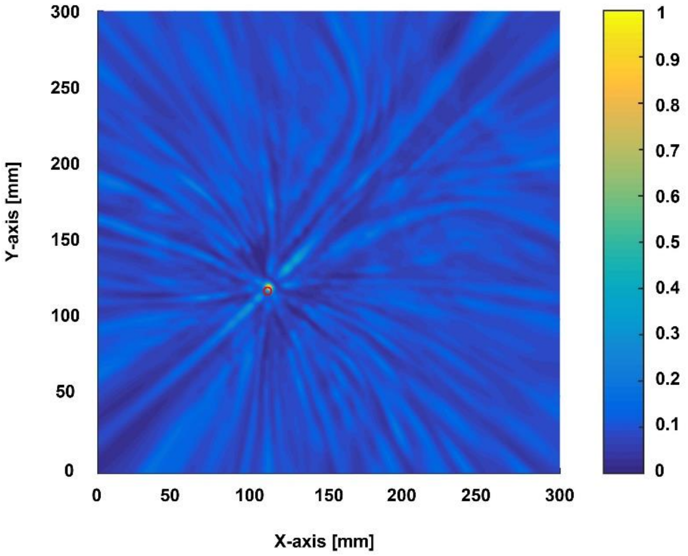

Fig. 8. Spatial spectrum obtained with F-MUSIC algorithm using six PZT wafers (P1, P2, P4, P5, P6, P8) (red ‘o’: actual damage).

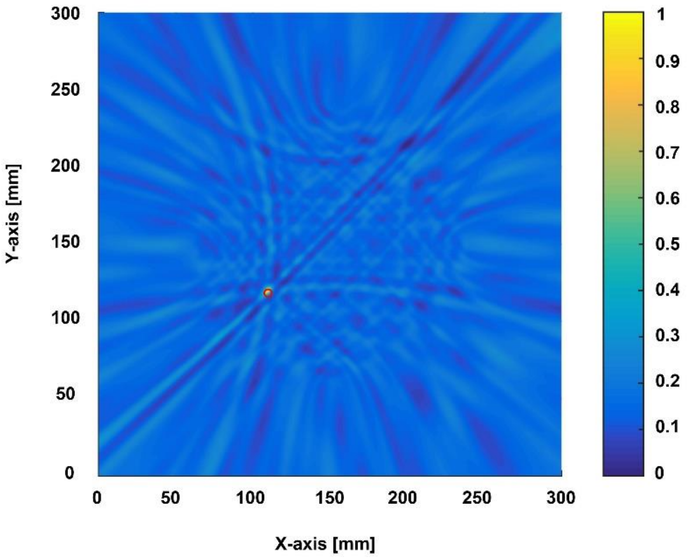

Fig. 9. Spatial spectrum obtained with F-MUSIC algorithm using four PZT wafers (P2, P4, P6, P8) (red ‘o’: actual damage).

Multiple Damage Sites

The capability of identifying multiple damage sites in the inspection region using F-MUSIC algorithm is studied. Two damage sites are included in the plate waveguide at (110 mm, 120 mm) and (190 mm, 180 mm), respectively. The spatial spectrum constructed using F-MUSIC algorithm is shown in **Fig. 10**, to observe quantitative match between identified and actual damage sites.

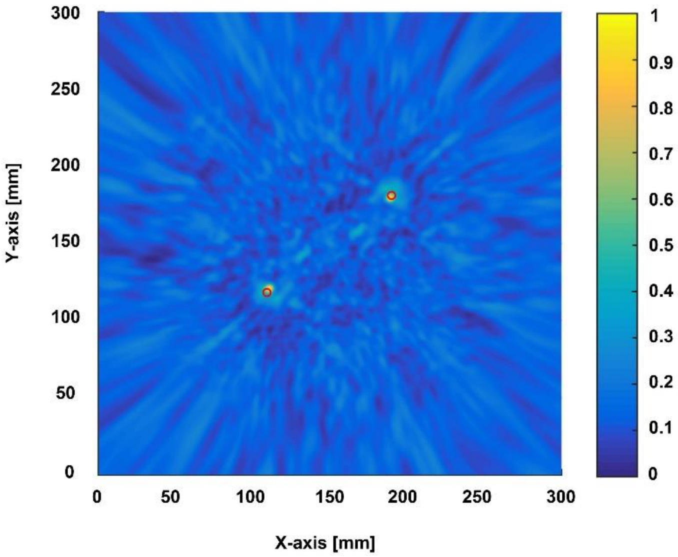

Fig. 10. Spatial spectrum obtained with F-MUSIC algorithm for a plate waveguide containing multi-damage (red ‘o’: actual damage).

4. Experimental Validation

Experimental validation is conducted. An aluminum plate (density: ρ=2700 kg/m^3; Young modulus: E=71 GPa; Poisson’s ratio: ν=0.33; dimension: 1000 mm × 1000 mm × 2 mm) is prepared, on which a sparse sensor network, consisting of eight PZT wafers (labelled as PZT-1, PZT-2, …, PZT-8), is surface-adhered, with respective locations indicated in **Fig. 11(a)**. The excitation is generated with a NI PXI-5412 arbitrary waveform generation unit, in the form of a 5-cycle Hanning-windowed tone-burst at the central frequency 200 kHz and amplified with a Ciprian US-TXP-3 linear power amplifier before applied in turn to each PZT wafer. The S_0 mode of Lamb waves are captured by remaining PZT wafers and then recorded with an Agilent MSOX 3014A oscilloscope at the sampling rate of 60 MHz. The experimental setup is shown schematically in **Fig.11(b)**.

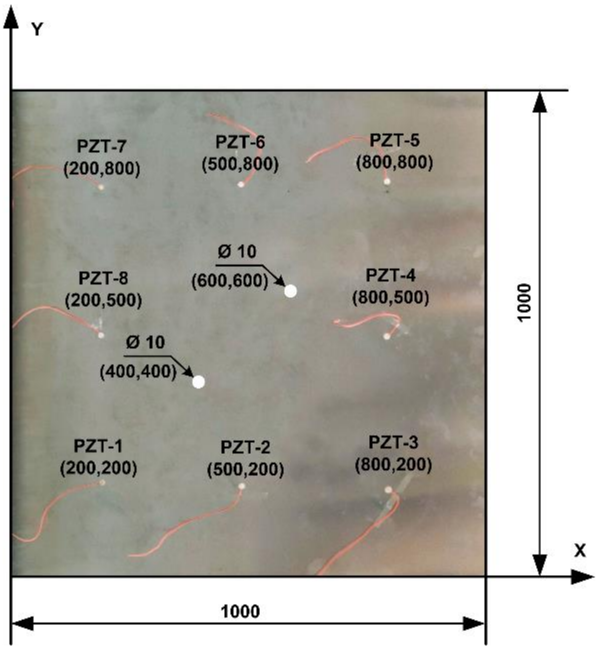

(a)

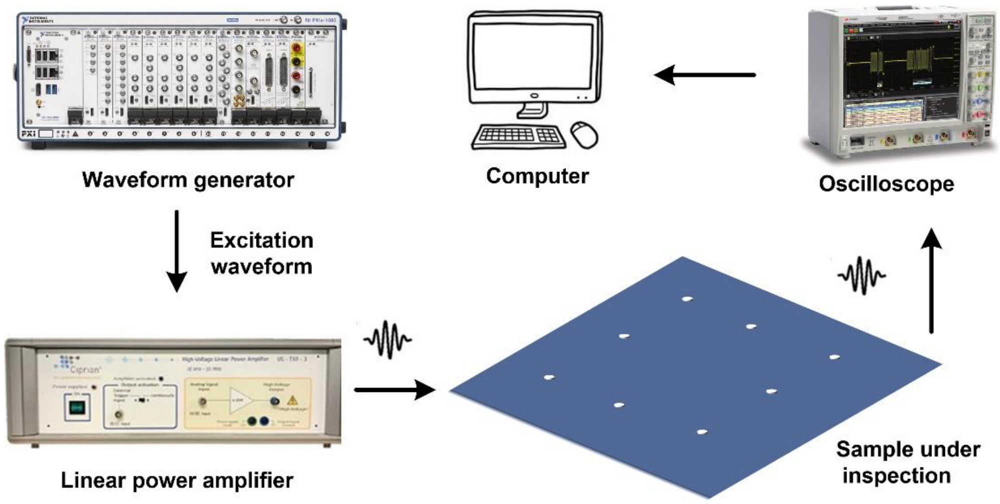

(b)

Fig. 11. (a) An aluminum plate with a surface-adhered sparse sensor network consisting of eight PZT wafers in experiment (all dimensions in mm); and (b) schematic of experimental set-up.

In line with simulation in Section 3, two damage scenarios are demonstrated in experiment. In the first case, a through-hole of a diameter of 10 mm is drilled at the location (400 mm, 400 mm) as a single damage case; after then multiple damage case C-II is studied by adding another through-hole of the same diameter at the location (600 mm, 600 mm). The F-MUSIC algorithm is applied to two damage cases to obtain the spatial spectra, in **Figs. 12(a)** and **(b)**, in which all damage sites are clearly depicted with high precise and image resolution.

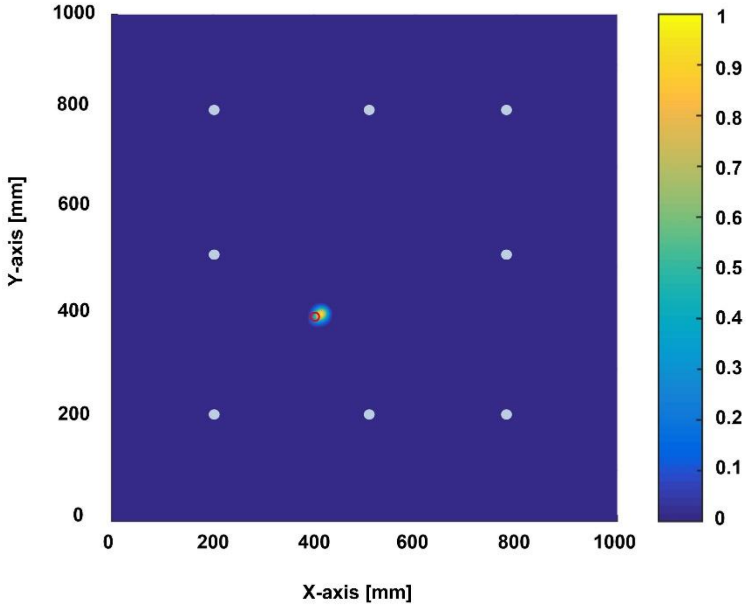

(a)

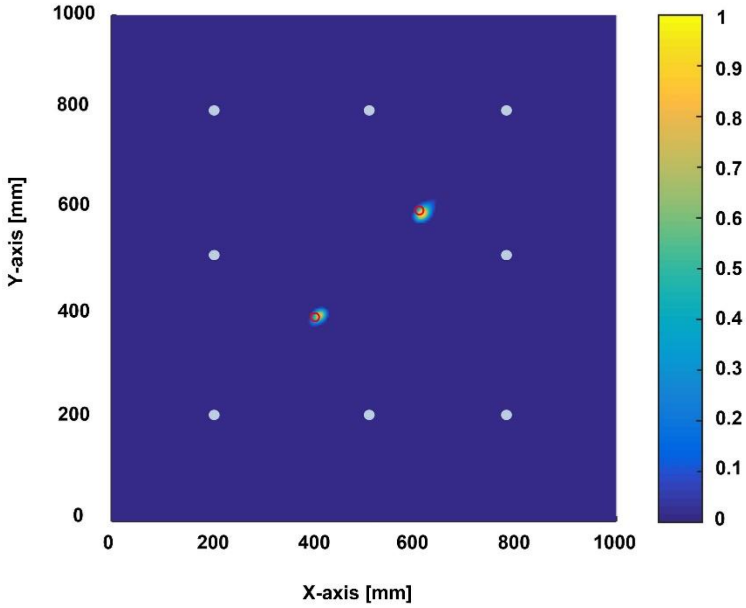

(b)

Fig. 12. Spatial spectra for (a) the single damage case (b) the multiple damage case (red 'o': actual damage).

5. Concluding Remarks

Aimed at exploiting merits of the Am-MUSIC algorithm (particularly its flexibility in configuring a sparse sensor network) that is earlier developed based on conventional MUSIC algorithms but surmounting deficiency that the Am-MUSIC algorithm still remains, a *frequency-domain MUSIC* (F-MUSIC) algorithm is developed, based on a multiple-damage-scattered wavefield model over the frequency domain. F-MUSIC avoids computationally expensive pixel-based calculation, and fuses rich information scattered in a broad band to enhance imaging precision. The algorithm is validated using simulation and experiment, and results articulate that effectiveness of F-MUSIC is not restricted by the quantity of damage, and with it the imaging precision is not sacrificed as a result of the use of a sparse sensor network.

Acknowledgments

The work was supported by a General Project (No. 51875492) and a Key Project (No. 51635008) received from the National Natural Science Foundation of China. Z Su acknowledges the support from the Hong Kong Research Grants Council via General Research Funds (Nos. 15202820, 15204419 and 15212417).

References

[1] X. Yang, K. Wang, P. Zhou, L. Xu, J. Liu, P. Sun, Z. Su, Ameliorated-multiple signal classification (Am-MUSIC) for damage imaging using a sparse sensor network, Mechanical Systems and Signal Processing, 163 (2022) 108154.
[2] M. Engholm, T. Stepinski, Direction of arrival estimation of Lamb waves using circular arrays, Structural Health Monitoring, 10 (2011) 467-480.
[3] Y. Zhong, S. Yuan, L. Qiu, Multiple damage detection on aircraft composite structures using near-field MUSIC algorithm, Sensors and Actuators A: Physical, 214 (2014) 234-244.
[4] S. Yuan, Y. Zhong, L. Qiu, Z. Wang, Two-dimensional near-field multiple signal classification algorithm–based impact localization, Journal of Intelligent Material Systems and Structures, 26 (2015) 400-413.
[5] P. Zabbal, G. Ribay, B. Chapuis, J. Jumel, Multichannel Multiple Signal Classification for dispersion curves extraction of ultrasonic guided waves, The Journal of the Acoustical Society of America, 143 (2018) EL87-EL92.
[6] C. Xu, J. Wang, S. Yin, M. Deng, A focusing MUSIC algorithm for baseline-free Lamb wave damage localization, Mechanical Systems and Signal Processing, 164 (2022) 108242.
[7] J.S. Hall, J.E. Michaels, Minimum variance ultrasonic imaging applied to an in situ sparse guided wave array, IEEE Transactions on Ultrasonics, Ferroelectrics, and Frequency Control, 57 (2010) 2311-2323.
[8] M. Liu, S. Chen, Z.Z. Wong, K. Yao, F. Cui, In situ disbond detection in adhesive bonded multi-layer metallic joint using time-of-flight variation of guided wave, Ultrasonics, 102 (2020) 106062.
[9] H. Jin, J. Yan, X. Liu, W. Li, X. Qing, Quantitative defect inspection in the curved composite structure using the modified probabilistic tomography algorithm and fusion of damage index, Ultrasonics, 113 (2021) 106358.
[10] R. Gorgin, Y. Luo, Z. Wu, Environmental and operational conditions effects on Lamb wave based structural health monitoring systems: A review, Ultrasonics, 105 (2020) 106114.
[11] H. Xu, L. Cheng, Z. Su, J.-L. Guyader, Identification of structural damage based on locally perturbed dynamic equilibrium with an application to beam component, Journal of sound and vibration, 330 (2011) 5963-5981.
[12] Y. Ren, L. Qiu, S. Yuan, Z. Su, A diagnostic imaging approach for online characterization of multi-impact in aircraft composite structures based on a scanning spatial-wavenumber filter of guided wave, Mechanical Systems and Signal Processing, 90 (2017) 44-63.
[13] F.-G. Yan, Y. Shen, M. Jin, Fast DOA estimation based on a split subspace decomposition on the array covariance matrix, Signal Processing, 115 (2015) 1-8.
[14] D. Kundu, Modified MUSIC algorithm for estimating DOA of signals, Signal Processing, 48 (1996) 85-90.
[15] Q. Bao, W. Hu, Q. Wang, A novel multi-site damage localization method based on near-field signal subspace fitting using uniform linear sensor array, Ultrasonics, 116 (2021) 106485.
[16] P. Zhou, X. Yang, Y. Su, J. Yang, L. Xu, K. Wang, L.-m. Zhou, Z. Su, Direct-write nanocomposite sensor array for ultrasonic imaging of composites, Composites Communications, 28 (2021) 100937.
[17] M. Engholm, T. Stepinski, Direction of arrival estimation of Lamb waves using circular arrays, Structural Health Monitoring, 10 (2010) 467-480.
[18] H. Yang, Y.J. Lee, S.K. Lee, Impact source localization in plate utilizing multiple signal classification, Proceedings of the Institution of Mechanical Engineers, Part C: Journal of Mechanical Engineering Science, 227 (2013) 703-713.
[19] H. Yang, T.J. Shin, S. Lee, Source location in plates based on the multiple sensors array method and wavelet analysis, Journal of Mechanical Science and Technology, 28 (2014) 1-8.

[20] S. Yuan, Q. Bao, L. Qiu, Y. Zhong, A single frequency component-based re-estimated MUSIC algorithm for impact localization on complex composite structures, Smart Materials and Structures, 24 (2015) 105021.
[21] Y. Zhong, S. Yuan, L. Qiu, Multi-impact source localisation on aircraft composite structure using uniform linear PZT sensors array, Structure and Infrastructure Engineering, 11 (2015) 310-320.
[22] Q. Bao, S. Yuan, F. Guo, L. Qiu, Transmitter beamforming and weighted image fusion–based multiple signal classification algorithm for corrosion monitoring, Structural Health Monitoring, 18 (2019) 621-634.
[23] H. Zuo, Z. Yang, C. Xu, S. Tian, X. Chen, Damage identification for plate-like structures using ultrasonic guided wave based on improved MUSIC method, Composite Structures, 203 (2018) 164-171.
[24] Q. Bao, S. Yuan, Y. Wang, L. Qiu, Anisotropy compensated MUSIC algorithm based composite structure damage imaging method, Composite Structures, 214 (2019) 293-303.
[25] Q. Bao, S. Yuan, F. Guo, A new synthesis aperture-MUSIC algorithm for damage diagnosis on complex aircraft structures, Mechanical Systems and Signal Processing, 136 (2020) 106491.
[26] S. Sundararaman, D.E. Adams, E.J. Rigas, Structural damage identification in homogeneous and heterogeneous structures using beamforming, Structural Health Monitoring, 4 (2005) 171-190.
[27] J. Yang, J. He, X. Guan, D. Wang, H. Chen, W. Zhang, Y. Liu, A probabilistic crack size quantification method using in-situ Lamb wave test and Bayesian updating, Mechanical Systems and Signal Processing, 78 (2016) 118-133.
[28] T. Gao, X. Liu, J. Zhu, B. Zhao, X. Qing, Multi-frequency localized wave energy for delamination identification using laser ultrasonic guided wave, Ultrasonics, 116 (2021) 106486.
[29] Y. Zhong, S. Yuan, L. Qiu, An improved two-dimensional multiple signal classification approach for impact localization on a composite structure, Structural Health Monitoring, 14 (2015) 385-401.